Available online at www.sciencedirect.com

ScienceDirect

Materials Chemistry and Physics 101 (2007) 291–296

MATERIALS CHEMISTRY AND PHYSICS

www.elsevier.com/locate/matchemphys

Preparation and characterization of ω-functionalized polystyrene–magnetite nanocomposites

Liming Jiang [a,*], Weilin Sun [a], Jungahn Kim [b]

[a] *Department of Polymer Science and Engineering, Zhejiang University, Hangzhou 310027, PR China*
[b] *Polymer Hybrids Center, Korea Institute of Science and Technology, Seoul 130-650, Republic of Korea*

Received 28 October 2004; received in revised form 7 May 2006; accepted 8 May 2006

Abstract

Magnetite (Fe_3O_4) nanoparticles were prepared by in situ precipitation and oxidation of ferrous ions in the presence of ω-functionalized polystyrenes having carboxylate, sulfonate, thiol, and thiolated groups. Based on the results for the orthogonal experimental design, both the ratio of the concentration of iron precursor to polymer and the reaction temperature were the major factors controlling the particle size and its shape morphology. By adjusting the reaction conditions, the iron oxide particle size can be effectively controlled in the range between 2 and 20 nm. The magnetite-based polymer composite was characterized by UV–vis spectroscopy, thermogravimetric analysis, transmission electron microscopy, and X-ray diffraction. Magnetization measurements revealed that the nanocomposite materials exhibit superparamagnetic behavior at room temperature.

Keywords: Magnetite; Nanocomposites; Synthesis; Magnetic properties

1. Introduction

In recent years, polymer-based magnetic nanocomposites have gained an increasing interest because of their potential applications [1,2]. A variety of functional polymers including derivatives of polystyrene [3–5], poly(vinylpyridine) [6,7], polyimine [8], poly(vinyl alcohol) [9–12], poly(pyrrole) [13], poly(aniline) [14,15], and poly(vinyl-pyrrolidone) [16] have been used in the preparation of nanocomposites. Recently, it has been reported that telechelic polystyrenes were successfully applied for the synthesis of nanosized cadmium sulfide particles [17]. However, little work has been reported on the use of terminally functionalized polymers as magnetic nanocomposite matrix.

In this article, we report a simple organic-phase synthesis of magnetite (Fe_3O_4) nanoparticles using ω-functionalized polystyrene as surfactant stabilizer affecting the morphology of the nanocomposite depending upon the ratio of Fe(II) ion to polymer and the reaction temperature. The formation of nanosized iron oxide particles within the polymer matrix was characterized using transmission electron microscopy (TEM) measurement, and the magnetic property of the composites was also examined briefly.

2. Experimental

2.1. Materials

All the chemicals as reagent were used without further purification. Ferrous chloride tetrahydrate ($FeCl_2{\cdot}4H_2O$) was obtained from Aldrich. Tetrahydrofuran (THF), toluene, *N*,*N*-dimethylformamide (DMF), methanol, and sodium hydroxide were purchased from J.T. Baker. The polymeric matrices used in this study include ω-sulfonate polystyrene ($PSSO_3H$, M_w 5 kDa), ω-thiolated polystyrene (PSSH or PSSLi, M_w 5 kDa), and ω-carboxylate polystyrene ($PSCO_2H$, M_w 39 kDa), which were synthesized by standard high vacuum techniques [18] and have a narrow molecular weight distribution ($M_w/M_n < 1.1$ determined by GPC).

2.2. Preparation of polymer–magnetite composites

The preparation of polystyrene–magnetite composites was performed as the following: a given amount of $FeCl_2{\cdot}4H_2O$ (25 mg) was dissolved in polymer/THF solution (12 g L^{-1}, 25 mL) under an argon atmosphere and the mixture was stirred for 6 h at room temperature or refluxing after injecting into aqueous NaOH (12.5N, 100 μL). Following the reaction, the solution was concentrated and then was isolated by precipitation in methanol. Drying under vacuum at 50 °C led to a powder sample.

---

[*] Corresponding author. Tel.: +86 571 87953727; fax: +86 571 87953727.
E-mail address: cejlm@zju.edu.cn (L. Jiang).

0254-0584/$ – see front matter © 2006 Elsevier B.V. All rights reserved.
doi:10.1016/j.matchemphys.2006.05.007

2.3. Measurements

UV–vis absorption spectra were obtained by a Hewlett-Packard 8453A Diode Array spectrophotometer. Raman spectra were recorded from 4000 to 200 cm^{-1} on a Nicolet Almega spectrometer. The X-ray diffraction (XRD) of the samples was obtained on a MacScience MXP18 diffractometer using Cu Kα radiation at wavelength $\lambda = 1.5405$ Å. Diffraction patterns were measured in 40 kV and 100 mA with 1° min^{-1} scan speed. The distances between peaks (d) were calculated according to Bragg's law. Transmission electron microscopic techniques (TEM, Philips CM) were employed to examine the morphology and the microstructure of composite samples. Thermogravimetric analysis (TGA) was carried out on a DuPont TGA 2950 in N_2 atmosphere between room temperature and 600 °C at a heating rate of 10 °C min^{-1}. Magnetic property of the composites was studied using a Physical Properties Measurement System (Model: PPM-9, Quantum Design) at fields ranging from −30 to 30 kOe and at temperatures from 5 to 300 K.

3. Results and discussion

3.1. Characterization of magnetic nanocomposites

Fig. 1 shows the UV–vis absorption spectra of as-prepared four samples using different ω-functionalized polystyrene matrices. Pure ω-functionalized PS samples were found to absorb below 300 nm; hence, the absorption between 300 and 450 nm can be attributed to the iron oxide nanoparticles embedded. It can be seen that the spectra a–c display broad peaks, which correspond to PSSH, PSSLi, and $PSSO_3H$-coated particles, respectively. Nevertheless, $PSCO_2H$-based composite has a different absorption fashion, in which an onset present at about 310 nm (d, Fig. 1). The observation was somewhat similar to that reported by Zhang and co-workers [19] In fact, the carboxyl terminated polystyrene seemed to be less effective at particle stabilization in this solution synthesis, which may be related to its higher molecular weight and/or the poor affinity of carboxyl groups to the oxide particle surface. It was also noted that the oxidation of ferrous ions carried out smoothly although under the protection of argon atmosphere. This suggests that the content of dissolved oxygen in the hydrophilic region of polymer matrices was high enough to the formation of oxide. We suspect that Fe(II) ions aggregated at the hydrophilic domains and in situ formed iron oxide particles were coated with polymer shell, and then dissolved in reaction media. Furthermore, the polymer chains would serve as templates to confine the growth of oxide particles. A set of comparison experiments proved that the PS matrix is necessary to prevent oxide particles from agglomeration caused by Van der Waals forces and magnetostatic interparticle interactions. Except THF, it was difficult to form a stable dispersion for other media such as toluene, DMF, and THF/MeOH, etc. However, the resultant powder product prepared in THF is readily soluble in toluene, chloroform, and DMF (~50 mg mL^{-1}), leading to a transparent brown organosol that remain stable after 6 months.

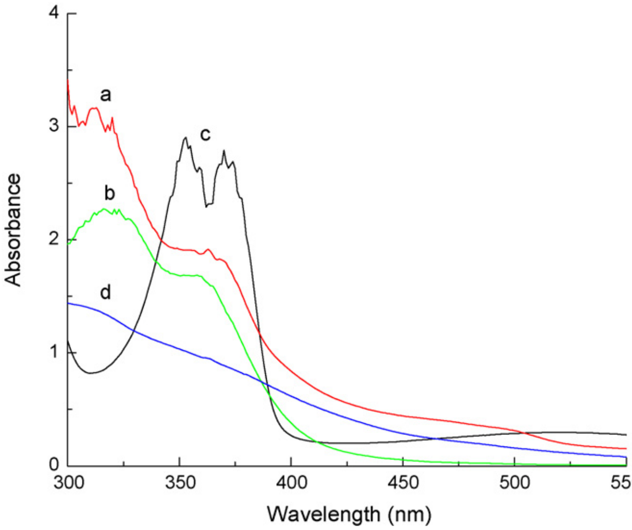

Fig. 1. UV–vis spectra of iron oxide–composites prepared within ω-functionalized PS matrices: (a) PSSH (5 kDa); (b) PSSLi (5 kDa); (c) $PSSO_3H$ (5 kDa), and (d) $PSCO_2H$ (39 kDa). Reaction conditions: polymer 300 mg; $FeCl_2{\cdot}4H_2O$ 0.2 mmol; NaOH (aq. 12.5N) 100 µL; 6 h at reflux under argon atmosphere.

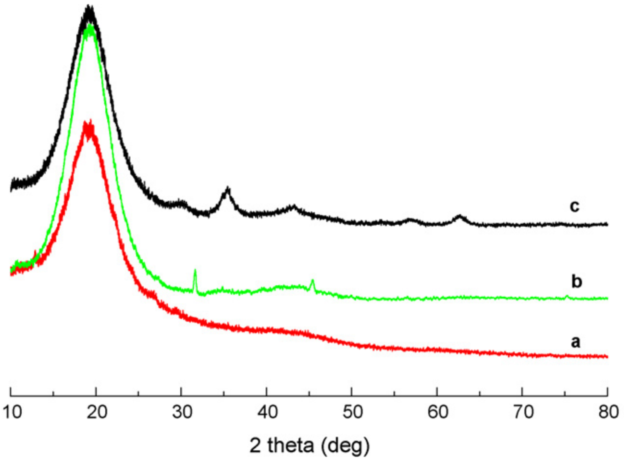

Fig. 2. X-ray powder diffraction patterns of Fe_3O_4–PSSLi composites prepared at different temperature: (a) 0 °C, (b) 23 °C, and (c) reflux. Reaction conditions: polymer 150 mg; THF 25 mL, $FeCl_2{\cdot}4H_2O$ 0.2 mmol; NaOH (aq. 12.5N) 100 µL; 6 h, Ar.

Typical XRD patterns of the as-synthesized nanocomposite are shown in Fig. 2. The patterns show a very broad peak at $d \approx 4.7$ Å, which is due to polystyrene and other diffraction peaks belonging to the polycrystalline iron oxide phase. As shown in Table 1, the d spacing values of the synthesized

Table 1
Diffraction angles (2θ) and d-spacing values (Å) corresponding to the peaks observed in the XRD pattern of the iron oxide–PSSLi composite sample

Peak	Diffraction angle (2θ)	d (exp)	d (ASTM data Fe_3O_4)[a]
1	29.73	3.0025	2.967
2	35.48	2.5280	2.532
3	42.7	2.1158	2.0993
4	53.56	1.7096	1.7146
5	56.64	1.6237	1.6158
6	62.76	1.4793	1.4845

[a] JCPDS card number: 19-629.

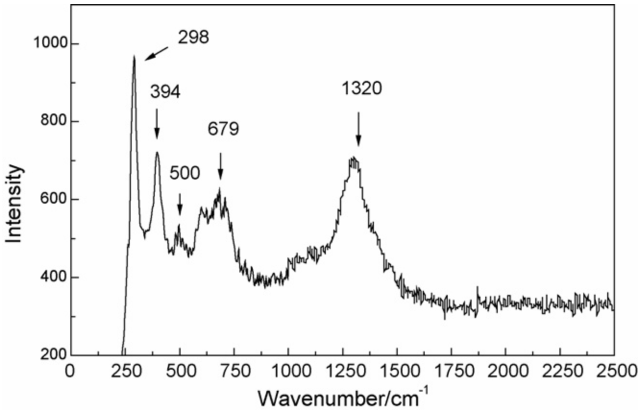

Fig. 3. Typical Raman spectrum of the synthesized nanocomposite.

iron oxide particles were close to standard JCPDS Fe_3O_4 data. In addition, Raman spectroscopy was also employed to further determine the nature of oxide cores (Fig. 3). The observed spectrum contained the Raman bands corresponding to Fe_3O_4, with a small quantity of the Raman bands for hematite (α-Fe_2O_3) [20,21]. These results indicate that the inorganic cores were mainly composed of Fe_3O_4.

Iron oxide particles synthesized at reflux are characterized by a well-defined X-ray diffraction pattern, suggesting formation of highly crystallized nanoparticles (Fig. 2). Conversely, the preparation performed at lower temperatures produced the particles with a low crystallinity. The mean particle size of 20 nm was deduced for the sample (Fig. 2c) by the Debye–Scherrer formula (mean crystallite size $D = 0.9\lambda/B\cos\theta$, where 0.9 is a dimensionless constant, $\lambda = 1.5405$ Å, B = broadening of width at the half-peak height in radians, and θ = Bragg's angle) [22]. On the other hand, the samples with a nominal iron oxide loading (<1 wt.%) did not display any peaks except that of polymer, likely due to the small particle sizes.

To investigate the influence of synthesis parameters on the size and shape morphology of the particles, a factorial design of experiments was established using the $L_9(3^4)$ orthogonal table [23]. This is a three-level three-factor system, in which values of the three levels of factors were chosen after performing a series of trial tests. In view of its comprehensive advantages, PSSLi was selected as a matrix for this orthogonal test. The experimental results and factor effects are listed in Table 2. TGA revealed the oxide content of 1.9–8.3 wt.% for these samples, which is slightly lower than that expected on the basis of the feed ratios because of the inevitable loss during preparation or handling of the materials. By a simple analysis to the data in Table 2, it can be found that the change in the amount of NaOH appears to have little influence on the particle size. However, the particle size was comparatively sensitive to an alteration of the Fe^{2+} feed ratio: the higher the feed ratio, the larger the particle size. This result implied that the nanoparticle size can be adjusted by changing the feed ratio of Fe(II) irons in a certain range.

The morphology and distribution of Fe_3O_4 nanoparticles in the hybrid composites were examined using transmission electron microscope (TEM). Some typical TEM images of the oxide–PSSLi composites are presented in Fig. 4. It can be seen that the Fe_3O_4 particles obtained at low feed ratio of Fe^{2+} was spherical and uniform in size with diameters of 1–2 nm (sample A4 in Fig. 4a). When the oxide content was raised in the composite, a higher density of particles and aggregates with larger sizes are clearly seen in Fig. 4c. For the sample A3, the particles displayed a flake-like shape with ~20 nm size (Fig. 4d), probably due to the effect of both the more amount of precursor Fe(II) ions and elevated reaction temperature. As shown in Fig. 4b, the nanoparticles prepared under adequate synthetic conditions were loosely distributed within the polymer matrix. Fig. 5 depicts the corresponding histogram of the size distribution obtained by measuring the diameter of 200 particles. It is apparent from the plot that the main distribution located the range between 6 and 10 nm.

3.2. Magnetic properties

The magnetization of ferromagnetic materials, such as magnetite and maghemite, is very sensitive to the microstructure of a particular sample. If a specimen consists of small particles, its total magnetization decreases with particle size, due to increasing dispersion on the exchange integral, and finally reaches the superparamagnetic state when each particle acts as a "spin"

Table 2
Results of three-factor three-level design[a]

No.	PSSLi (mg)	$FeCl_2 \cdot 4H_2O$ (mmol)	NaOH (12.5N, μL)	Temperature (°C)	Fe_3O_4/composite (wt.%) (TGA)[b]	Particle size (nm)
A1	150	0.1	100	0	4.5 (4.9)	8–15
A2	150	0.2	250	r.t.	8.3 (9.3)	15–20
A3	150	0.15	150	Reflux	7.1 (7.2)	19.8[c]
A4	450	0.1	250	Reflux	1.9 (1.7)	1–2
A5	450	0.2	150	0	3.1 (3.3)	3–5
A6	450	0.15	100	r.t.	2.1 (2.5)	1–2
A7	300	0.1	150	r.t.	2.3 (2.5)	3–5
A8	300	0.2	100	Reflux	4.8 (4.9)	7.2[c]
A9	300	0.15	250	0	3.4 (3.7)	5–8

[a] PSSLi, FW = 5000; THF 25 mL; Ar atmosphere for 6 h.

[b] TGA: thermogravimetric analysis. The data in parentheses are wt.% of iron oxide expected from feed ratios.

[c] Calculated from XRD data by the Debye–Scherrer formula.

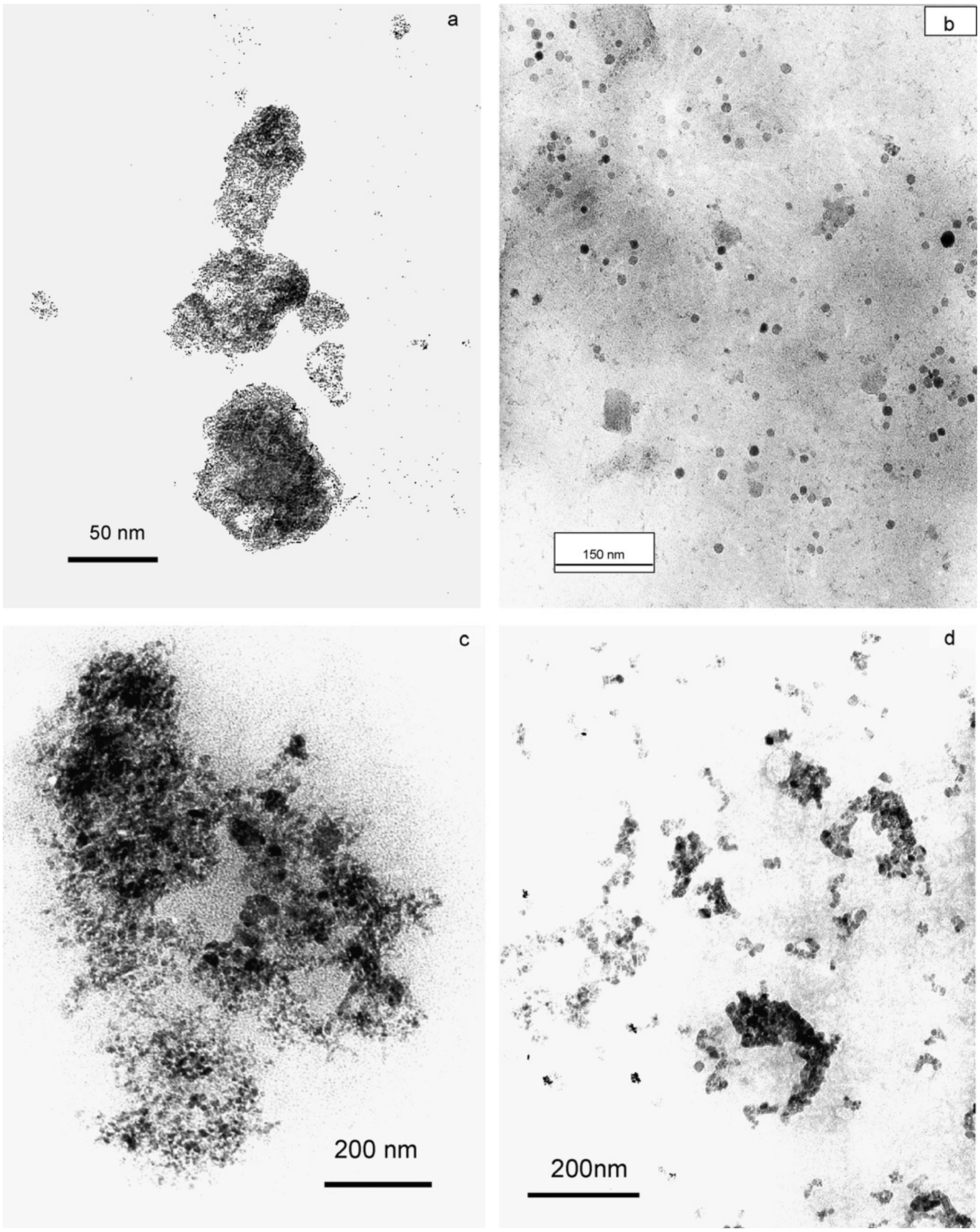

Fig. 4. TEM micrographs of as-prepared Fe_3O_4–composite samples: (a) A4, (b) A8, (c) A2, and (d) A3 (see: Table 2).

with suppressed exchange interaction between the particles [24]. Fig. 6 shows the magnetization of a nanocomposite sample (A3) as a function of applied magnetic field at room temperature. The composite material exhibited extremely small hysteresis loop and coercivity. This lack of hysteresis and coercivity is characteristic of superparamagnetic particles or some single-domain particles [25,26]. For this sample with magnetite loading of ~7%, the saturation magnetization (σ_s) was about 6.3 emu g^{-1} at 30 kG. When expressed per gram of magnetite in the nanocomposites, σ_s equals ~90 emu g^{-1} of Fe_3O_4. Apparently, the larger distribution and smaller size of particles decreases σ_s considerably due to relaxation effects of spins on the surface atoms [27].

The temperature dependence of the magnetization was measured with use of zero-field cooling (ZFC) and field cooling (FC) procedures in an applied magnetic field of 100 Oe between 5 and 300 K (Fig. 7). Above 50 K the magnetization decreases with increasing temperature in both ZFC and FC cases. At lower temperatures the magnetization increases monotonically with decreasing temperature for the FC, whereas the ZFC magnetization passes through a maximum at ~40 K, which can be associated with the blocking temperature [27].

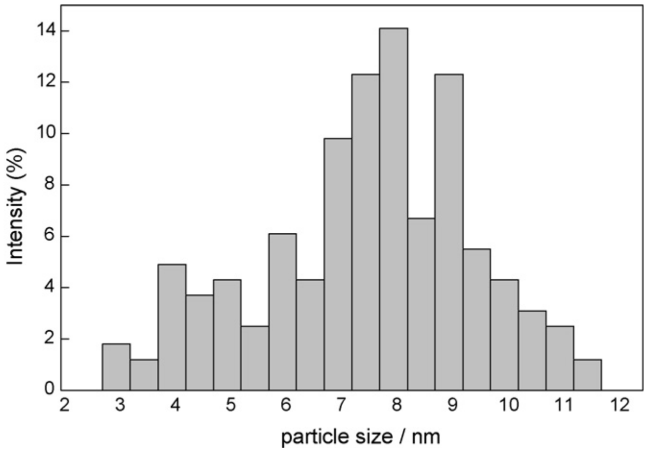

Fig. 5. A histogram of particle size distribution of sample A8 (see: Table 2 and Fig. 4b).

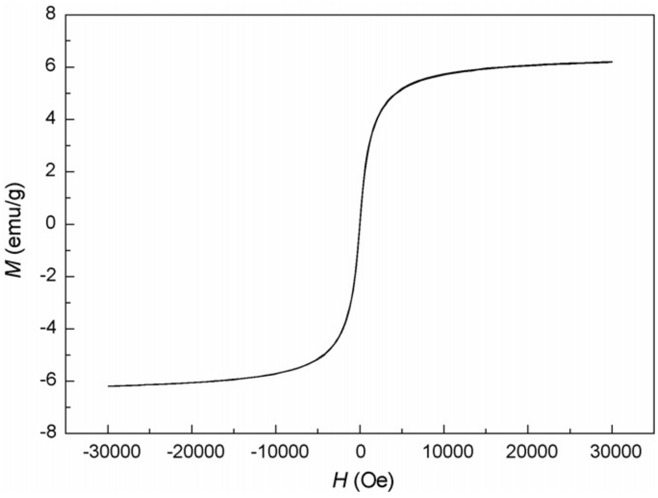

Fig. 6. Magnetization of PSSLi-based magnetite composite as a function of applied magnetic field at room temperature (sample A3 in Table 2).

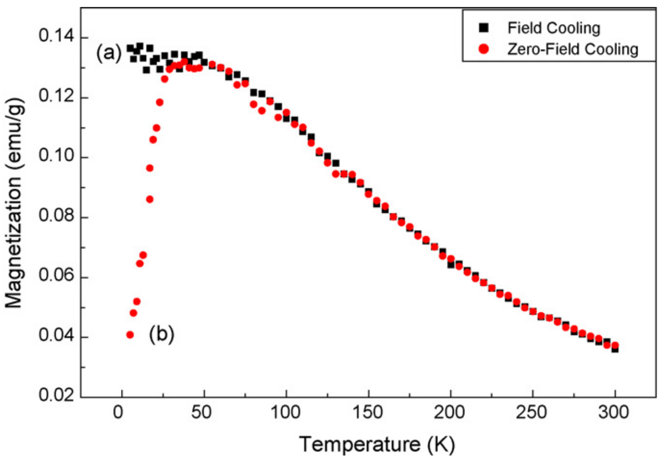

Fig. 7. Magnetization vs. temperature for PSSLi-coated magnetite nanocomposite (sample A3 in Table 2) at $H = 100$ Oe: (a) field cooled; (b) zero-field cooled.

4. Conclusions

Nanometer-sized Fe_3O_4–composites have been successfully prepared by in situ precipitation and oxidation of ferrous ions within ω-functionalized polystyrene matrices in the organic media. By changing the Fe(II) precursor feed ratio and reaction temperature, the particle size of in situ formed iron oxide can be tuned in the range of 2–20 nm. The particle morphology and crystallinity were also dependent on the synthetic parameters. The resultant hybrid materials would be expected to have some potential applications due to their easy availability and specially stability in organosol state.

Acknowledgments

This work was financially supported by both the National Natural Science Foundation of China (no. 20274036) and the Korea Foundation for Advanced Studies (KFAS) International Scholar Exchange Fellowship Program (2002–2003). The main studies were completed in Prof. Jungahn Kim's laboratory, Korea Institute of Science and Technology (KIST).

References

[1] D.L. Leslie-Pelecky, R.D. Rieke, Chem. Mater. 8 (1996) 1770.
[2] J. Tajada, X.X. Zhang, E. Kroll, X. Bohigas, R.F. Ziolo, J. Appl. Phys. 87 (2000) 8008.
[3] X. Ding, Z. Sun, W. Zhang, Y. Peng, A.S.C. Chan, P. Li, Colloid. Polym. Sci. 278 (2000) 459.
[4] R.F. Ziolo, E.P. Giannelis, B.A. Weinstein, M.P. O'Horo, N.B. Ganguly, V. Mehrotra, M.W. Russell, D.R. Haffman, Science 257 (1992) 219.
[5] N.A.D. Burke, H.D.H. Stver, F.P. Dawson, Chem. Mater. 14 (2002) 4762.
[6] J. Ramos, A. Millán, F. Palacio, Polymer 41 (2000) 8641.
[7] L. Chen, W.J. Yang, C.Z. Yang, J. Mater. Sci. 32 (1997) 3571.
[8] C. Castro, A. Millan, F. Palacio, J. Mater. Chem. 10 (2000) 1945.
[9] J. Lee, T. Isobe, M. Senna, J. Colloid Interf. Sci. 177 (1996) 490.
[10] A.E. Varfolomeev, D.Yu. Godovskii, G.A. Kapustin, A.V. Volkov, M.A. Moskvina, JETP Lett. 67 (1998) 39.
[11] R. Vijaya Kumar, Yu. Koltypin, Y.S. Cohen, Y. Cohen, D. Aurbach, O. Palchik, I. Felner, A Gedanken, J. Mater. Chem. 10 (2000) 1125.
[12] H. Lin, Y. Watanabe, M. Kimura, K. Hanabusa, H. Shirai, J. Appl. Polym. Sci. 87 (2002) 1239.
[13] M.D. Butterworth, S.A. Bell, S.P. Armes, A.W. Simpson, J. Colloid Interf. Sci. 183 (1996) 91.
[14] M. Kryszewski, J.K. Jeszka, Synth. Met. 94 (1998) 99.
[15] B.Z. Tang, Y. Geng, J.W.Y. Lam, B. Li, X. Jing, X. Wang, F. Wang, A.B. Pakhomov, X.X. Zhang, Chem. Mater. 11 (1999) 1581.
[16] K.S. Suslick, M. Fang, T. Hyeon, J. Am. Chem. Soc. 118 (1996) 11960.
[17] J. Kim, S.S. Kim, K.H. Kim, Y.H. Jin, S.M. Hong, S.S. Hwang, B.-G. Cho, D.Y. Shin, S.S. Im, Polymer 45 (2004) 3527.
[18] M. Morton, L.J. Fetters, Rubber Chem. Technol. 48 (1975) 359.
[19] N.J. Cherepy, D.B. Liston, J.A. Lovejoy, H. Deng, J.Z. Zhang, J. Phys. Chem. B 102 (1998) 770.
[20] J. Dünnwald, A. Otto, Corros. Sci. 29 (1989) 1167.
[21] T. Ohtsuka, K. Kubo, N. Sato, Corrosion 42 (1986) 476.
[22] H. Klug, L. Alexander, X-ray Diffraction Procedures for Polycrystalline and Amorphous Materials, John Wiley & Sons, New York, 1962, pp. 491–538.

[23] O.L.K. Davies, Design and Analysis of Industrial Experiments, 2nd ed., Longman Group Limited, London and New York, 1978.
[24] C. Sudakar, G.N. Subbanna, T.R.N. Kutty, J. Mater. Chem. 12 (2002) 107.
[25] B.H. Sohn, R.E. Cohen, Chem. Mater. 9 (1997) 264.
[26] S. Mann, J.P. Hannington, J. Colloid Interf. Sci. 22 (1988) 326.
[27] J.K. Vassiliou, V. Mehrotra, M.W. Russell, E.P. Giannelis, R.D. McMichael, R.D. Shull, R.F. Ziolo, J. Appl. Phys. 73 (1993) 5109.